Visible-wavelength multiphoton activation confocal microscopy

AUTHOR NAMES.

Toshiki Kubo[1, 2], Kenta Temma[1, 2], Kazunori Sugiura[3], Hajime Shinoda[3], Kai Lu[3], Nicholas Isaac Smith[4], Tomoki Matsuda[3], Takeharu Nagai[3,5], and Katsumasa Fujita[1, 2, 5]*

AUTHOR ADDRESS

[1]Department of Applied Physics, Osaka University, 2-1 Yamadaoka, Suita, Osaka 565-0871, Japan.

[2]Advanced Photonics and Biosensing Open Innovation Laboratory, AIST-Osaka University, Osaka University, 2-1 Yamadaoka, Suita, Osaka 565-0871, Japan

[3]The Institute of Scientific and Industrial Research (SANKEN), Osaka University, 8-1 Mihogaoka, Ibaraki, Osaka 567-0047, Japan

[4]Immunology Frontier Research Center, Osaka University, 3-1 Yamadaoka, Suita, Osaka 565-0871, Japan

[5]Transdimensional Life Imaging Division, Institute for Open and Transdisciplinary Research Initiatives, Osaka University, 2-1 Yamadaoka, Suita, Osaka 565-0871, Japan

ABSTRACT.

Nonlinear optical effects modify the point spread function (PSF) in laser scanning microscopy and have been utilized to enhance the spatial resolution in three-dimensions. In this paper, we propose the use of visible-wavelength two-photon excitation to activate negatively switching reversibly photo-switchable fluorescent proteins (RSFPs) to introduce nonlinear relationships between the distribution of excitation light and the fluorescence emission. Single-photon excitation following the two-photon induced photo-activation provides a PSF corresponding to the cube of the excitation intensity distribution and achieves imaging properties equivalent to that using third-order nonlinear optical effects. We experimentally confirmed several species of negatively switching RSFPs can be activated by two-photon excitation in the wavelength range of 530-560 nm. We applied the cubic PSF imaging to the observation of HeLa cells stained by Skylan-NS to confirm the improvement of the spatial resolution and the image contrast in confocal scanning microscopy.

Keywords

fluorescence, nonlinear, reversibly photo-switchable fluorescent proteins, visible-wavelength two-photon excitation, confocal detection, super-resolution microscopy, cell imaging

Introduction

Nonlinear optical effects induced by focused laser light localize within an area smaller than the focus spot because of the nonlinear relationships between excitation and the optical effects. Laser scanning microscopy utilizing nonlinear optical effects, such as SHG microscopy[1], multiphoton excitation microscopy[2], and coherent Raman microscopy[3,4] can provide a spatial resolution in three-dimensions and suppress the out-of-focus signal that degrades the image contrast. Therefore, the nonlinear optical microscopy has been utilized for high-contrast volumetric imaging of cell and tissue structures in thick specimens. In addition, using a short-wavelength light, the nonlinear optical microscopy can realize a spatial resolution beyond the diffraction limit of visible light, which has been demonstrated in biological imaging[5-7].

There have been several attempts to create such nonlinear relationships without nonlinear optical effects, in particular, to improve the spatial resolution of confocal fluorescence microscopy. The methods are based on the use of fluorescent probes which have two states with different capabilities of fluorescence emission. Those probes exhibit nonlinear relationships between excitation and emission intensity via photo-switching between fluorescence-on and -off states by light absorption. The fluorescence emission of such probes is generated by two-step photon absorption: the first absorption switches the off state to the on state (activation), and the second absorption excites probes in the on state, after which they can emit fluorescence. The two absorptions do not need to overlap in time, therefore, the resulting emission distribution for such probes is the square of the intensity distribution of the irradiation laser spot when the wavelengths for activation and excitation are the same, even though the absorption process is linear. Such a fluorescent probe has been first realized by combining two fluorescent molecules. One of them acts as a donor and the other as an accepter of Förster resonance energy transfer (FRET)[8-11]. The

use of photo-induced charge separation between the two molecules was also proposed[12]. Another type of probe with on- and off- fluorescence states are reversibly photo-switchable fluorescent proteins (RSFPs). The nonlinear fluorescence response of RSFPs has been utilized in laser scanning microscopy where it improved spatial resolution[13]. Moreover, near-infrared (NIR) two-photon excitation has been applied to RSFPs, where the distribution of activation efficiency is quadratically dependent on the intensity distribution of the laser spot. Therefore, the distribution of the fluorescence emission is proportional to the third power of the intensity distribution of laser spots. The property of NIR two-photon activation (NIR2PA) has been studied[14,15] and also applied to laser scanning microscopy in order to improve the image contrast and the imaging depth[16,17].

In this paper, we developed a super-resolution imaging technique by showing the possibility of combining multi-photon activation of negatively switching RSFPs, using visible-wavelength light, and confocal detection. We refer to this technique as vMAC (visible-wavelength multi-photon activation confocal) microscopy. The use of visible-wavelength two-photon excitation[7] localizes the activation of negatively switching RSFPs within a volume smaller than the laser spot. By detecting the activated RSFPs using one-photon excitation confocal microscopy, we can achieve super-resolution imaging by evoking the fluorescence emission with a 3rd order nonlinear dependency on the intensity distribution of irradiation laser spots. We first report and discuss the photo-activation of RSFPs by using visible-wavelength two-photon excitation and then demonstrate how it can be applied to super-resolution imaging of biological samples.

Activating RSFPs by visible-wavelength two-photon excitation

Figure 1 shows a schematic of the principle of the resolution improvement in vMAC microscopy (Figure 1(a) and (d)) and comparisons with confocal microscopy by NIR2PA and one-photon excitation (1PE) (Figure 1(b) and 1(e)) and conventional 1PE confocal microscopy (Figure 1(c) and 1(f)). In vMAC microscopy, RSFPs are set to the off state initially and activated by visible-wavelength two-photon absorption. Then, RSFPs at the on-state are excited by one-photon absorption at a visible wavelength. In confocal microscopy, as a result, the fluorescence distribution is given as the product of the square of the intensity distribution of the activation laser spot and that of the excitation laser spot, resulting in the highly-localized fluorescence emission in the laser spot, which is similar to inducing a 3rd order nonlinearity in the excitation-emission relation.

The effective PSFs were calculated to compare the spatial resolutions between the imaging modes as shown in Figure 1 (d) – (f). The effective PSF of vMAC microscopy was calculated by the product of three components: the square of the intensity distribution of the activation laser focus, the intensity distribution of the excitation laser focus, and the detection PSF convolved with the sensitivity distribution of the detector. The intensity distributions and the detection PSF were calculated by using vectorial diffraction theory[18]. We assumed circular or random polarization in the calculation. We described the detail of the calculation including those for other imaging modes in the supporting information. Figure 1 (d) – (f) indicate that the spatial resolution of vMAC microscopy is higher than those of 1PE confocal and NIR2PA with 1PE confocal microscopy, respectively. Although NIR2PA includes nonlinear excitation (similar to vMAC microscopy), the improvement of the spatial resolution is limited due to the long wavelengths used for activation.

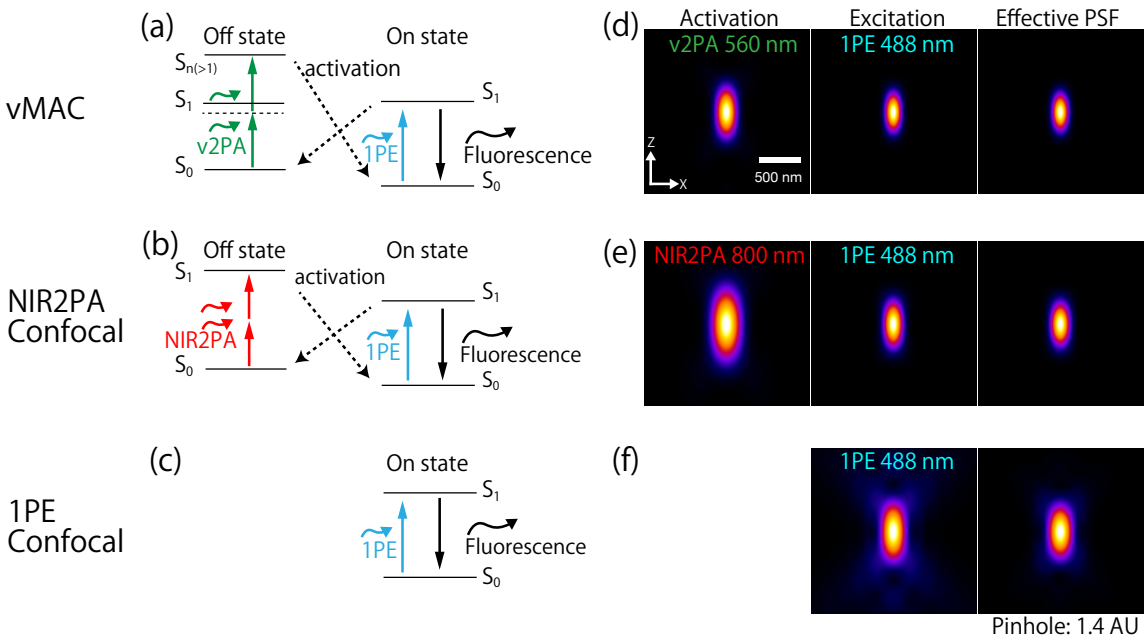

Figure 1. Energy diagrams of reversibly photo-switchable fluorescent protein (RSFP) under (a) visible-wavelength two-photon activation (v2PA) and one-photon excitation for visible-wavelength multi-photon activation confocal (vMAC), and (b) NIR two-photon activation (NIR2PA) and one-photon excitation (1PE). (c) An energy diagram of conventional fluorescent protein under one-photon excitation. (d)-(f) Simulated distribution of activation, fluorescence emission, and effective PSF of the three types of confocal microscopies, respectively.

To confirm that visible-wavelength two-photon excitation can activate RSFPs, we measured the relationship between the irradiation intensity of visible-wavelength pulsed light and switching efficiency. We used a wavelength-tunable pulsed laser beam to investigate the capability of two-photon activation with different wavelengths. We irradiated four different wavelengths of 530, 540, 550, and 560 nm on four different species of negatively switching RSFPs: rsEGFP2[19], Skylan-NS[20], Dronpa[21], and rsGamillus-S[22] in our experiments. Those RSFPs can be activated by one-photon absorption of UV or violet light, such as 405 nm laser.

We estimated the switching efficiency from fluorescence intensity measured by a confocal microscope with 488 nm laser for excitation. The confocal microscope was also equipped with an optical parametric oscillator (OPO) pumped by a NIR femtosecond pulsed laser as a light source for visible-wavelength activation. The two laser beams are focused at the same position and temporally modulated to realize the fluorescence measurement after activation of RSFPs with different intensities of the pulsed light. In our measurement, we used fixed HeLa cells expressing the RSFPs in their actin filament, where activated RSFPs can then remain at the same locations during irradiation and detection. Initially, the RSFPs in the sample were set to the off state by widefield illumination using blue light with a wavelength range of 460-495 nm because the RSFPs spontaneously and gradually switch to the on state[20,23]. To avoid repeating measurements at the same position, we measured fluorescence intensities at positions separated by at least 1 Airy Unit of the 488 nm laser focus. Since the cell samples are not homogeneous, the fluorescence signal reflects not only the amount of photo-activation by pulsed laser but also the distribution of RSFPs. In order to obtain the distribution of probe concentration and to calculate the switching efficiency, we measured the fluorescence intensities of the same points after activating by widefield irradiation of UV light with a range of 330-385 nm. In addition, we also estimated the fluorescence intensity from RSFPs at the off state. Since the RSFPs at the off state still emit weak fluorescence, the fluorescence signal obtained by the 488 nm laser after activation also contains the signal from off-state RSFPs. We measured the fluorescence intensity of the off-state RSFPs following light irradiation using blue light, then subtracted that from the signal after activation to compensate for the effect of the off-state RSFPs when estimating the switching efficiency. Please see the supporting information for the details of this procedure.

Figure 2 shows the optical setup for the measurement of switching efficiency. We used an OPO (Inspire HF100, Spectra-Physics) pumped by a NIR femtosecond pulsed laser (Mai-Tai, Spectra-Physics) to activate the fluorescent proteins. The pulse width and repetition rate of the resultant visible pulsed laser are 200 fs and 80 MHz, respectively. An acousto-optic modulator (AOM, AOM-402AF1, IntraAction) was used to temporally modulate the pulsed laser light. For the 1PE light source, we used a continuous wave (CW) laser with a wavelength of 488 nm (LuxXpulse 488-200, Omicron) which can be electrically modulated. After being expanded and collimated by the beam expanders, the laser beams were focused at the same position on the sample by a silicone-oil immersion objective lens (UPlanSApo, ×60 NA 1.30, Olympus). Laser spots were scanned on samples by a single-axis galvanometric mirror (M2ST, GSI Lumonics) in the x direction and a three-axis piezo stage (P-561.3CD, Physik Instrumente) in the y and z directions, respectively. The piezo stage was placed on a sample stage of an inverted microscope (IX-71, Olympus), equipped with a mercury lamp, a blue excitation filter set (U-MNIB3, Olympus), and a UV excitation filter set (U-MWU2, Olympus) for widefield illumination. The fluorescence signal from samples was collected by the same objective lens and focused on a pinhole placed in front of a photomultiplier tube (PMT, H7422-40, Hamamatsu) for fluorescence detection. The fluorescence signal was separated from the irradiation light by the combination of a short-pass filter (FF01-533/SP-25, Semrock), a notch filter (NF03-488E-25, Semrock), a long-pass filter (FEL0500, Thorlabs), and a short-pass filter (FF01-546/SP, Semrock).

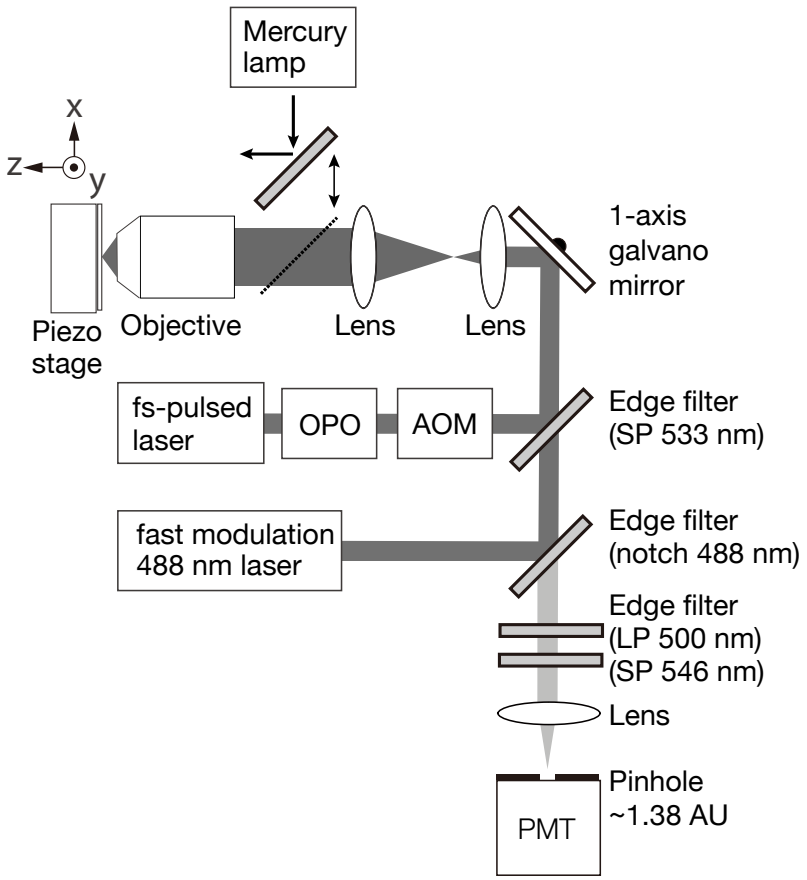

Figure 2. Optical setup. OPO, AOM, SP, LP, PMT, and AU represents Optical Parametric Oscillator, acousto-optic modulator, short-pass filter, long-pass filter, photo-multiplier tube, and Airy Unit, respectively.

Figure 3 shows the switching efficiency under irradiation of visible-wavelength pulsed laser light for activation of the four different RSFPs, which were measured as the fluorescence signal obtained at different activation intensities. The intensities of the widefield illuminations were set at 1.2 W/cm^2 and 9.2 W/cm^2 for UV and blue, respectively. The exposure time of the widefield illuminations was set at 5 s and 30 s for UV and blue, respectively. The intensities of the lasers were set in a range of 0.1-10 MW/cm^2 for the pulsed laser, and at 1.32 kW/cm^2 for the 488 nm laser, respectively. The exposure time of the lasers at each pixel was set to 0.5 ms for each.

We investigated the capability of two-photon activation by the pulsed laser with wavelengths of 530, 540, 550, and 560 nm. As shown in Figure 3, the switching efficiency of the four RSFPs was found to exhibit a second-order nonlinear response to the activation intensity of the pulsed laser, depending on the wavelength. This result indicates that the activation is induced by two-photon excitation of these RSFPs. In some results, the slope of the curve is smaller than 2 at low and high activation intensities, which is due to the small amount of activated protein and saturation of activation, respectively. In the measurement using Skylan-NS, Dronpa, and rsGamillus-S, we found that pulsed laser irradiation at shorter wavelengths (e.g. 530 or 540) did not increase the fluorescence signal by the following 488 nm excitation, which is presumably due to photobleaching by 1PE of visible pulsed laser light, as discussed later. The results also show that the shortest wavelength of the pulsed laser which enables to obtain 2nd order nonlinearity of the switching efficiency against puled laser intensity is different for each RSFP.

In order to compare the v2PA with NIR2PA, the response of the switching efficiency of the RSFPs was measured using an 800 nm pulsed laser for the activation. 800 nm pulsed laser was directly introduced into the microscope optics without going through the OPO. In this experiment, the pulse width and the repetition rate of the pulsed laser are 100 fs and 80 MHz, respectively. The switching efficiency of rsEGFP2, Skylan-NS, and Dronpa showed quadratic responses to the irradiation intensity even at 800 nm. The switching efficiency of NIR2PA at the same activation intensity was slightly higher than that of v2PA, which could be attributed to the larger activation volume compared to v2PA.

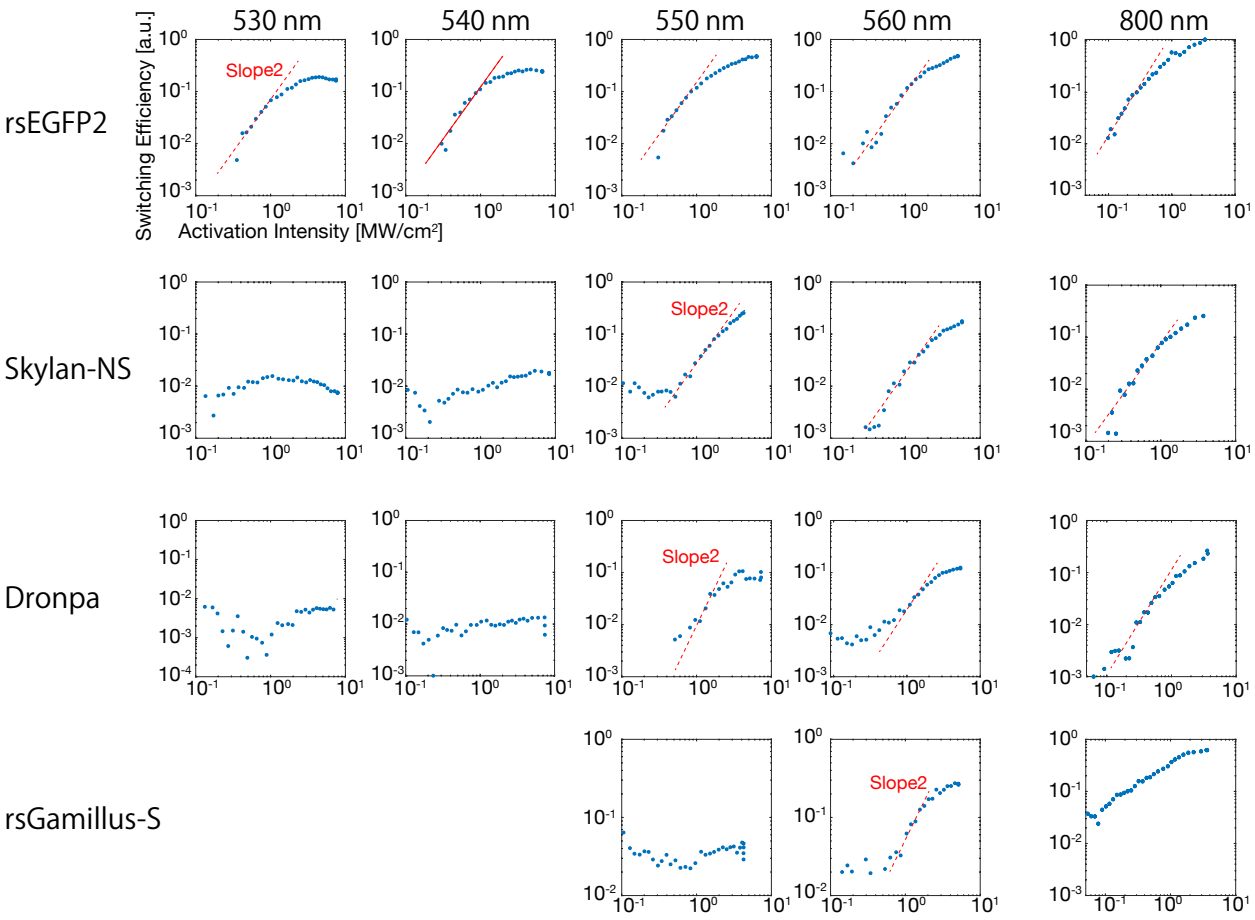

Figure 3. Switching efficiency of rsEGFP2, Skylan-NS, Dronpa, and rsGamillus-S with the pulsed laser at wavelengths of 530, 540, 550, 560, and 800 nm, respectively. At certain wavelengths for each RSFPs, we did not see the fluorescence signal contributed by activation from the pulsed laser irradiation. The efficiency response curves of rsGamillus-S with 530 nm and 540 nm pulsed irradiation could not be plotted in log-log scale because many negative values are obtained, presumably due to photo-bleaching by one-photon excitation by the pulsed laser made the intensity lower than the "off" 488 nm image.

Demonstration of super-resolution imaging by vMAC microscopy

To evaluate the capability of visible-wavelength multi-photon activation for super-resolution imaging, we observed cell samples by vMAC microscopy. The optical setup of vMAC microscopy was the same as that for measuring the switching efficiency and is shown in Figure 2. We adopted Skylan-NS as the fluorescent probe for the imaging as it provided the most fluorescence signal out of the four RSFPs that we measured. The activation wavelength of 560 nm was adopted since the range of switching efficiency where 2nd order nonlinearity appeared was larger than that of 550 nm activation.

Figure 4 shows the imaging procedure in vMAC microscopy. At each pixel of an image, the sample is irradiated by the 488 nm CW laser light for 8 ms to deactivate Skylan-NS in the focus spot (i.e. ensure the sample is in the off-state). After an interval of 0.05 ms for avoiding a temporal overlap of deactivation and activation, the 560 nm pulsed laser was illuminated for 2 ms for activation. Then, the 488 nm CW laser light was irradiated for 2 ms to excite fluorescence after an interval of 0.05 ms. This activation-excitation cycle was repeated three times in order to obtain enough signal for imaging.

In our experiment, the intensities of 560 nm pulsed and 488 nm CW light were 1 MW/cm^2 and 13 kW/cm^2, respectively. The intensity of the pulsed laser was set to a value high enough to induce two-photon activation but not saturate. The intensity of the 488 nm laser was set to an intensity at which Skylan-NS did not show obvious photobleaching after imaging. An exposure time of 8 ms was required to switch most Skylan-NS in a single spot to the off state by 488 nm laser light. The fluorescence signal measured while irradiating 488 nm light for 2 ms was used to construct the images. As mentioned above, the fluorescence signal includes signals from both on- and off-state RSFPs, which contribute to 3rd order nonlinear and linear fluorescence imaging, respectively. To

extract the 3rd order nonlinear image, we obtained a linear fluorescence signal at the irradiation of 488 nm light. Then the linear signal was subtracted from the fluorescence signal after activation by 560 nm to reconstruct super-resolved fluorescence images.

The x-y and x-z images of the cells obtained in both vMAC and linear confocal modes are shown in Figure 5(a), (b), (f), and (g). Figure 5(c) and (d) show the line profiles of the image of thin structures. In Figure 5(a) and (f), we applied a green color scale to the negative values to show the effect of over subtraction. The values are within the noise level and were seen in a small number of pixels, showing the subtraction process did not produce significant artifacts. The FWHM of the result of Gaussian fitting was about 136 nm and 226 nm. In theory, FWHMs of the simulated image of an actin filament (Figure S5 in the supporting information) in the x-y direction were 135 nm and 210 nm for vMAC and linear confocal microscopy, respectively, which are similar to the results in the experiments. Figure 5(e) shows the comparison of the line profiles of the image of two filaments within a distance of about 200 nm, which is in between the theoretical resolution of the vMAC and conventional confocal microscopy. The fiber-like structures were resolved in vMAC microscopy but not in linear confocal microscopy as expected from the theoretical investigation. The resolution improvement was also clearly seen in the z direction. Figure 5(h) shows the line profile of the image of a thin filament structure for z-direction by vMAC microscopy, and Figure 5(i) shows the comparison of the line profile of the same position in the image obtained by conventional confocal microscopy. The FWHM of the line profile in vMAC microscopy was about 325 nm, which is similar to the theoretical resolution of 314 nm estimated from the simulated image of vMAC microscopy shown in Figure S5 in the supporting information. The line profiles also revealed the high image contrast for the reduced background signal in vMAC microscopy, compared with conventional confocal microscopy.

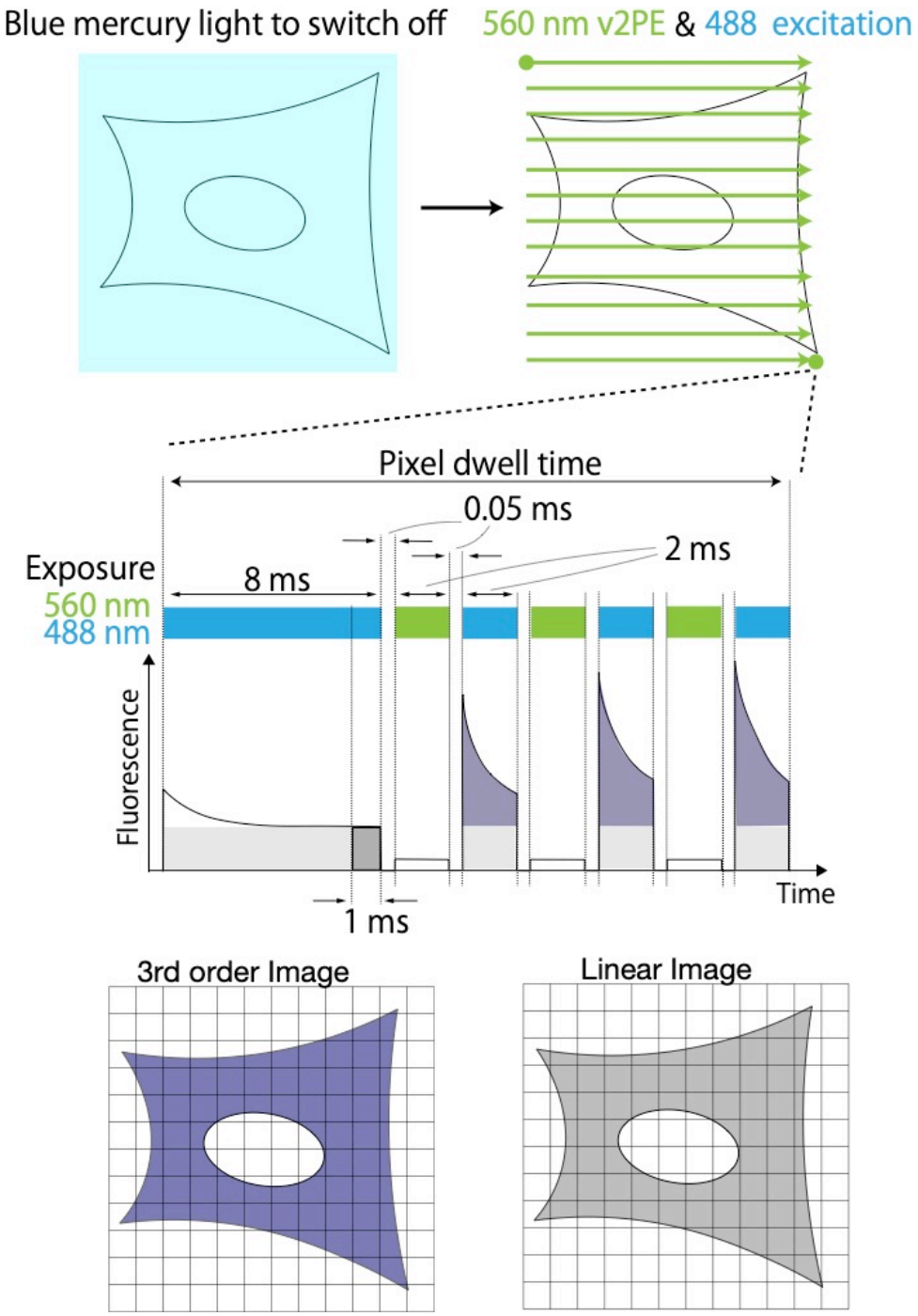

Figure 4. The imaging procedure in vMAC microscopy used for imaging the cells stained with Skylan-NS.

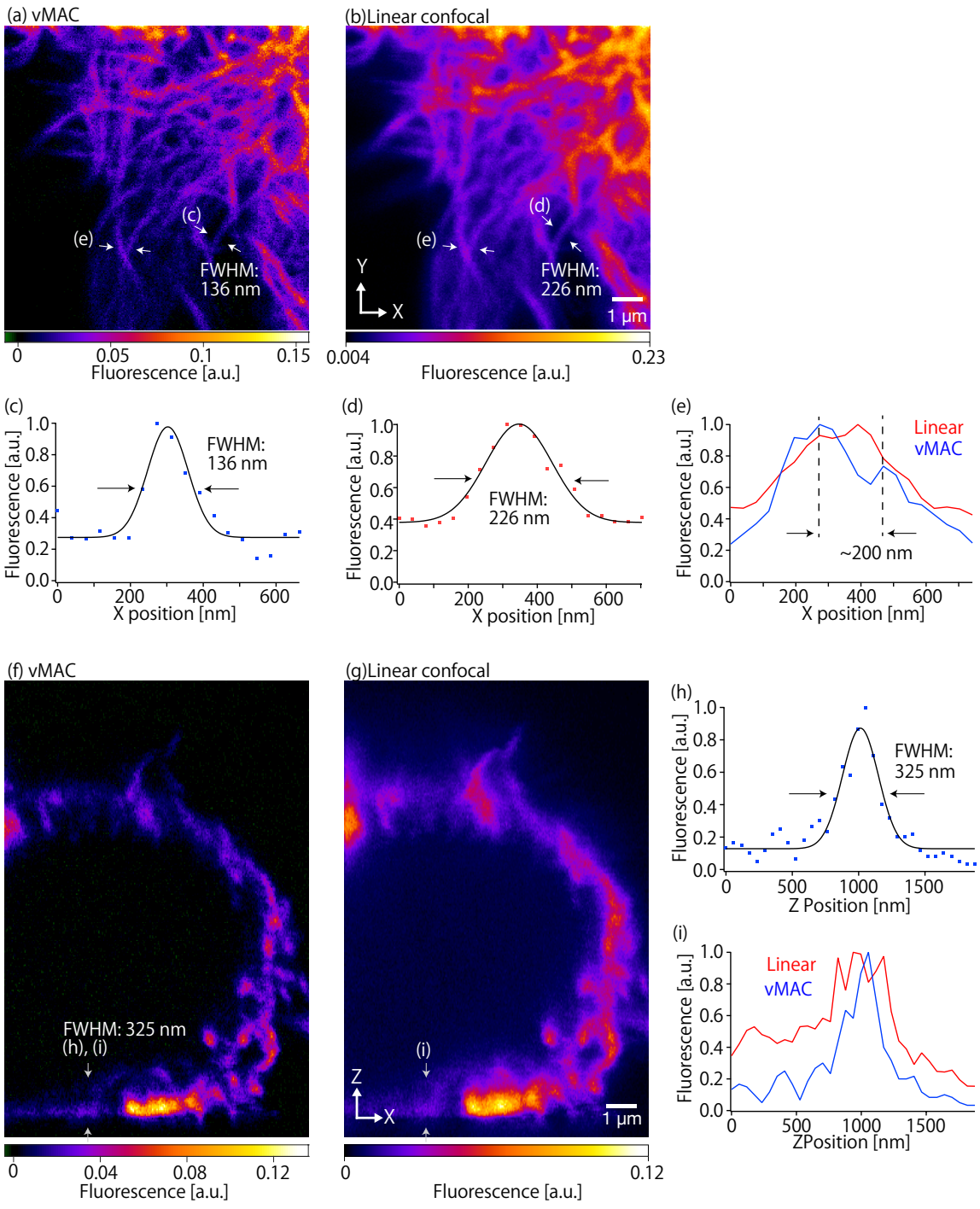

Figure 5. Fluorescence images of living HeLa cells expressing Skylan-NS on their actin filament which were obtained by (a)(f) vMAC microscopy and (b)(g) linear confocal microscopy. The line profiles were taken to evaluate and compare the spatial resolution between vMAC and linear confocal microscopy. The profiles are taken along the lines made by each pair of facing arrows

drawn in the images. The line profiles in (c), (d), and (h) were taken across thin structures in the image to estimate the practical measured FWHM. The line profiles are normalized by their respective maximum values. The line profiles in (e) and (i) were taken at the same positions of the image (a)(b) and (f)(g), respectively. Pixel size was 39 nm, 39 nm, and 58 nm in x, y, and z direction, respectively.

Conclusion and Discussion

In this research, we demonstrated the activation of negatively switching RSFPs using visible-wavelength two-photon excitation. The switching efficiency of Skylan-NS, Dronpa, rsEGFP2, and rsGamillus-S under pulsed excitation at 560 nm was proportional to the square of the activation intensity, which indicated that the activation of RSFPs occurred by the two-photon process. The intracellular imaging by vMAC microscopy showed the improvement of spatial resolution in 3D, which confirmed the capability of vMAC microscopy for super-resolution imaging.

The switching efficiencies of the RSFPs by v2PA are dependent on the wavelength of the activation light. Irradiation of pulsed light with a relatively shorter wavelength did not increase fluorescence under excitation by 488 nm light. However, even in such cases, we found that photobleaching occurred under high-intensity irradiation of activation light. This would be caused by one-photon absorption of the pulsed laser after two-photon activation. Since those activation wavelengths are close to the bandgap of activated RSFPs, the strong pulsed laser light would be absorbed and rapidly bleached the RSFPs. In addition, the absorption spectra of the four RSFPs (Figure S6) support the above discussion. In the measurement of RSFPs with a longer peak wavelength of the absorption spectra, photobleaching occurred at the longer wavelength.

Compared to NIR2PA, the switching efficiency in v2PA can be estimated to be smaller because of the following reasons. The wavelength for v2PA is close to the absorption wavelength of the

RSFPs in the on-state, resulting in deactivation by one-photon absorption immediately after activation and less fluorescence emission in confocal imaging using 488 nm. NIR2PA can also deactivate the RSFPs, however, the efficiency can be smaller since it is induced by two-photon absorption. The other reason is the difference in the activation volume as mentioned in the above section. We calculated the amount of fluorescence emission using two-photon activation at wavelengths of 530 nm, 560 nm, and 800 nm under confocal imaging using 488 nm for excitation. To estimate the signal amount, we firstly calculated the intensity distribution of fluorescence emission as shown in the middle column of Figure 1 (d), (e), and (f) with assuming a uniformly distributed sample was activated. After normalizing by their respective peak intensity, we accumulated the intensity over the calculated area. The signal amount using 800 nm activation was 1.79 and 1.98 times larger than 530 and 560 nm, respectively. Even if the difference in effective focal volume is taken into account, the required activation intensity in v2PA is comparable with NIR2PA. Considering that shorter wavelength two-photon excitation generally induces more photobleaching[24-26], v2PA is considered to be more damaging than NIR2PA.

Since the resolution improvement in our technique only relies on the nonlinearity of the fluorescence emission against the intensity distribution of the laser spots, the required configuration of the optics is simple. The observation does not suffer from out of focus signal, and therefore the resultant image exhibits a high image contrast similar to two-photon excitation microscopy. Therefore, our technique is suitable for three-dimensional imaging of a relatively thick specimen with high spatial resolution, which can be an advantage compared to other super-resolution imaging techniques. Moreover, since only simple image processing is required to improve the spatial resolution, real-time super-resolution imaging is available. However, although

vMAC microscopy is a nonlinear imaging technique, it is not suitable for imaging deep parts of tissue samples because of the use of visible laser light for fluorescence activation and excitation.

Three-photon excitation (3PE) also shows fluorescence intensity proportional to the cube of the excitation intensity. 3PE uses long wavelengths around 900, 1300, or 1700 nm wavelength according to the color of the fluorescent probes[27]. Although the longer excitation wavelength in 2PE enables the observation of deep parts of a specimen, the spatial resolution is lower. 3PE using a relatively shorter wavelength, such as 900 nm, can only reach a resolution similar to one-photon excitation using visible wavelength[28]. In vMAC microscopy, the sequential excitation of two-photon activation and one-photon excitation offers the 3rd order imaging property with an irradiation laser power similar to NIR two-photon excitation, which is typically smaller than intensities required for 3PE. However, vMAC imaging requires a longer imaging time than 3PE imaging due to the sequential excitation. In the current implementation, live cell imaging by vMAC microscopy is limited by sample motion. Although our observation of actin filaments showed no significant motion artifacts, observations of fast-moving samples by vMAC microscopy may suffer from motion artifacts.

The use of v2PA might cause significant phototoxicity since it utilizes absorption in the DUV region. However, in our experiment, we found that the photobleaching during 488 nm exposure was dominant and required to set the measurement condition not to bleach the RSFPs. In order to avoid the photobleaching by 488 nm, it was required to use a low excitation intensity with a long exposure time, which made the imaging speed of vMAC microscopy slow. The development of RSFPs which shows tolerance to photo-bleaching will be required to shorten the exposure for switching off. To improve the temporal resolution, parallelization via multifocus scanning techniques[29, 6] is available.

A higher-order nonlinear image can be achieved by the use of saturation in visible multiphoton activation. Since saturated two-photon excitation inherently has 4th order nonlinearity[30], the combination of saturation of visible-wavelength multiphoton activation and one-photon excitation offers a higher-order nonlinearity in the illumination-signal relation that can further improve the spatial resolution in 3D.

ASSOCIATED CONTENT

AUTHOR INFORMATION

Corresponding Author

Katsumasa Fujita - Department of Applied Physics, Osaka University, 2-1 Yamadaoka, Suita, Osaka 565-0871, Japan.; Advanced Photonics and Biosensing Open Innovation Laboratory, AIST-Osaka University, Osaka University, 2-1 Yamadaoka, Suita, Osaka 565-0871, Japan; Transdimensional Life Imaging Division, Institute for Open and Transdisciplinary Research Initiatives, Osaka University, 2-1 Yamadaoka, Suita, Osaka 565-0871, Japan; Email: fujita@ap.eng.osaka-u.ac.jp

ACKNOWLEDGMENT

This work was partially supported by Japan Science and Technology Agency under Grant Number JPMJCR15N3. This study was also partially supported by JST COI-NEXT under Grant Numbers JPMJPF2009, and Japan Society for the Promotion of Science under Grant Number 18H05410. A part of this work was performed under the Cooperative Research Program of the "Network Joint Research Center for Materials and Devices: Dynamic Alliance for Open Innovation Bridging Human, Environment and Materials".

Supporting Information.

The Supporting Information is available free of charge via the Internet at http://pubs.acs.org

The calculation of effective PSFs, the estimation of switching efficiency, the procedure of the switching efficiency measurements, the simulation of the image of actin filaments, and the absorption spectra of the reversibly photo-switchable fluorescent proteins (RSFPs) that were used in the switching efficiency measurements are included in the Supporting Information. (PDF)

REFERENCES

(1) Sheppard, C. J.; Kompfner, R. Resonant Scanning Optical Microscope. *Appl. Opt.* **1978**, *17* (18), 2879–2882.

(2) Denk, W.; Strickler, J. H.; Webb, W. W. Two-Photon Laser Scanning Fluorescence Microscopy. *Science* **1990**, *248* (4951), 73–76.

(3) Zumbusch, A.; Holtom, G. R.; Xie, X. S. Three-Dimensional Vibrational Imaging by Coherent Anti-Stokes Raman Scattering. *Phys. Rev. Lett.* **1999**, *82* (20), 4142–4145.

(4) Freudiger, C. W.; Min, W.; Saar, B. G.; Lu, S.; Holtom, G. R.; He, C.; Tsai, J. C.; Kang, J. X.; Sunney Xie, X. Label-Free Biomedical Imaging with High Sensitivity by Stimulated Raman Scattering Microscopy. *Science*. 2008, pp 1857–1861. https://doi.org/10.1126/science.1165758.

(5) Yamanaka, M.; Saito, K.; Smith, N. I.; Arai, Y.; Uegaki, K.; Yonemaru, Y.; Mochizuki, K.; Kawata, S.; Nagai, T.; Fujita, K. Visible-Wavelength Two-Photon Excitation Microscopy for Fluorescent Protein Imaging. *J. Biomed. Opt.* **2015**, *20* (10), 101202.

(6) Oketani, R.; Suda, H.; Uegaki, K.; Kubo, T.; Matsuda, T.; Yamanaka, M.; Arai, Y.; Smith, N.; Nagai, T.; Fujita, K. Visible-Wavelength Two-Photon Excitation Microscopy with Multifocus Scanning for Volumetric Live-Cell Imaging. *J. Biomed. Opt.* **2019**, *25* (1), 1–5.

(7) Kubo, T.; Temma, K.; Smith, N. I.; Lu, K.; Matsuda, T.; Nagai, T.; Fujita, K. Hyperspectral Two-Photon Excitation Microscopy Using Visible Wavelength. *Opt. Lett.* **2021**, *46* (1), 37–40.

(8) Hänninen, P. E.; Lehtelä, L.; Hell, S. W. Two- and Multiphoton Excitation of Conjugate-Dyes Using a Continuous Wave Laser. *Opt. Commun.* **1996**, *130* (1), 29–33.

(9) Schönle, A.; Hänninen, P. E.; Hell, S. W. Nonlinear Fluorescence through Intermolecular Energy Transfer and Resolution Increase in Fluorescence Microscopy. *Ann. Phys.* **1999**, *8* (2), 115–133.

(10) Chen, J.; Cheng, Y. Far-Field Superresolution Imaging with Dual-Dye-Doped Nanoparticles. *Optics Letters*. 2009, p 1831. https://doi.org/10.1364/ol.34.001831.

(11) Xu, F.; Wei, L.; Chen, Z.; Min, W. Frustrated FRET for High-Contrast High-Resolution Two-Photon Imaging. *Opt. Express* **2013**, *21* (12), 14097–14108.

(12) Mochizuki, K.; Shi, L.; Mizukami, S.; Yamanaka, M.; Tanabe, M.; Gong, W.-T.; Palonpon, A. F.; Kawano, S.; Kawata, S.; Kikuchi, K.; Fujita, K. Nonlinear Fluorescence Imaging by Photoinduced Charge Separation. *Jpn. J. Appl. Phys.* **2015**, *54* (4), 042403.

(13) Ingaramo, M.; York, A. G.; Andrade, E. J.; Rainey, K.; Patterson, G. H. Two-Photon-like Microscopy with Orders-of-Magnitude Lower Illumination Intensity via Two-Step Fluorescence. *Nat. Commun.* **2015**, *6*, 8184.

(14) Schneider, M.; Barozzi, S.; Testa, I.; Faretta, M.; Diaspro, A. Two-Photon Activation and Excitation Properties of PA-GFP in the 720–920-Nm Region. *Biophys. J.* **2005**, *89* (2), 1346–1352.

(15) Hartwich, T. M. P.; Subach, F. V.; Cooley, L.; Verkhusha, V. V.; Bewersdorf, J. Determination of Two-Photon Photoactivation Rates of Fluorescent Proteins. *Phys. Chem. Chem. Phys.* **2013**, *15* (36), 14868–14872.

(16) Zhu, X.; Kao, Y.-T.; Min, W. Molecular-Switch-Mediated Multiphoton Fluorescence Microscopy with High-Order Nonlinearity. *J. Phys. Chem. Lett.* **2012**, *3* (15), 2082–2086.

(17) Kao, Y.-T.; Zhu, X.; Xu, F.; Min, W. Focal Switching of Photochromic Fluorescent Proteins Enables Multiphoton Microscopy with Superior Image Contrast. *Biomed. Opt. Express* **2012**, *3* (8), 1955–1963.

(18) Richards, B.; Wolf, E.; Gabor, D. Electromagnetic Diffraction in Optical Systems, II. Structure of the Image Field in an Aplanatic System. *Proc. R. Soc. Lond. A Math. Phys. Sci.* **1959**, *253* (1274), 358–379.

(19) Grotjohann, T.; Testa, I.; Reuss, M.; Brakemann, T.; Eggeling, C.; Hell, S. W.; Jakobs, S. RsEGFP2 Enables Fast RESOLFT Nanoscopy of Living Cells. *Elife* **2012**, *1*, e00248.

(20) Zhang, X.; Zhang, M.; Li, D.; He, W.; Peng, J.; Betzig, E.; Xu, P. Highly Photostable, Reversibly Photoswitchable Fluorescent Protein with High Contrast Ratio for Live-Cell Superresolution Microscopy. *Proc. Natl. Acad. Sci. U. S. A.* **2016**, *113* (37), 10364–10369.

(21) Habuchi, S.; Ando, R.; Dedecker, P.; Verheijen, W.; Mizuno, H.; Miyawaki, A.; Hofkens, J. Reversible Single-Molecule Photoswitching in the GFP-like Fluorescent Protein Dronpa. *Proc. Natl. Acad. Sci. U. S. A.* **2005**, *102* (27), 9511–9516.

(22) Shinoda, H.; Lu, K.; Nakashima, R.; Wazawa, T.; Noguchi, K.; Matsuda, T.; Nagai, T. Acid-Tolerant Reversibly Switchable Green Fluorescent Protein for Super-Resolution Imaging under Acidic Conditions. *Cell Chem Biol* **2019**, *26* (10), 1469-1479.e6.

(23) Zhang, X.; Chen, X.; Zeng, Z.; Zhang, M.; Sun, Y.; Xi, P.; Peng, J.; Xu, P. Development of a Reversibly Switchable Fluorescent Protein for Super-Resolution Optical Fluctuation Imaging (SOFI). *ACS Nano* **2015**, *9* (3), 2659–2667.

(24) Herz, J.; Siffrin, V.; Hauser, A. E.; Brandt, A. U.; Leuenberger, T.; Radbruch, H.; Zipp, F.; Niesner, R. A. Expanding Two-Photon Intravital Microscopy to the Infrared by Means of Optical Parametric Oscillator. *Biophys. J.* **2010**, *98* (4), 715–723.

(25) Marchant, J. S.; Stutzmann, G. E.; Leissring, M. A.; LaFerla, F. M.; Parker, I. Multiphoton-Evoked Color Change of DsRed as an Optical Highlighter for Cellular and Subcellular Labeling. *Nat. Biotechnol.* **2001**, *19* (7), 645–649.

(26) Drobizhev, M.; Makarov, N. S.; Tillo, S. E.; Hughes, T. E.; Rebane, A. Two-Photon Absorption Properties of Fluorescent Proteins. *Nat. Methods* **2011**, *8* (5), 393–399.

(27) Horton, N. G.; Wang, K.; Kobat, D.; Clark, C. G.; Wise, F. W.; Schaffer, C. B.; Xu, C. In Vivo Three-Photon Microscopy of Subcortical Structures within an Intact Mouse Brain. *Nat. Photonics* **2013**, *7* (3), 205–209.

(28) Hell, S. W.; Bahlmann, K.; Schrader, M.; Soini, A.; Malak, H. M.; Gryczynski, I.; Lakowicz, J. R. Three-Photon Excitation in Fluorescence Microscopy. *J. Biomed. Opt.* **1996**, *1* (1), 71–74.

(29) Bewersdorf, J.; Pick, R.; Hell, S. W. Multifocal Multiphoton Microscopy. *Opt. Lett.* **1998**, *23* (9), 655–657.

(30) Oketani, R.; Doi, A.; Smith, N. I.; Nawa, Y.; Kawata, S.; Fujita, K. Saturated Two-Photon Excitation Fluorescence Microscopy with Core-Ring Illumination. *Opt. Lett.* **2017**, *42* (3), 571–574.

For Table of Contents Use Only

Title: Visible-wavelength multiphoton activation confocal microscopy

Author: *Toshiki Kubo, Kenta Temma, Kazunori Sugiura, Hajime Shinoda, Kai Lu, Nicholas Isaac Smith, Tomoki Matsuda, Takeharu Nagai, and Katsumasa Fujita*

A brief synopsis:

Visible-wavelength two-photon excitation has been utilized for photoactivation of reversibly photo-switchable fluorescent proteins. Combined with successive one-photon excitation and confocal detection, super-resolution fluorescence imaging of living cells was achieved by nonlinear point-spread function engineering.